Ab initio studies of structural, vibrational, and electronic properties of durene crystals and molecules

F. Ortmann, K. Hannewald, and F. Bechstedt
Institut für Festkörpertheorie und -optik, Friedrich-Schiller-Universität, Max-Wien-Platz 1, 07743 Jena, Germany and European Theoretical Spectroscopy Facility (ETSF)
(Received 22 December 2006; published 31 May 2007)

We present an *ab initio* analysis of durene in its gas phase as well as in its crystalline phase by means of density-functional theory. The structural ground-state parameters are determined for three exchange and correlation functionals and compared with experimental data. The crystalline phase is found to be influenced not only by van der Waals bonds but also by weak intermolecular C-H$\cdots\pi$ hydrogen bonds. The vibrational frequencies and eigenmodes are calculated within the local-density approximation and a one-to-one comparison between both phases is presented. Supplemented by a group-theoretical analysis, we identify infrared-active as well as Raman-active modes and calculate the corresponding IR spectra. The electronic energy levels of durene molecules, as well as the band structure of durene crystals, are calculated from the Kohn-Sham approach. Special emphasis is put on the origin of the large bandwidths and dispersion anisotropy in durene crystals. Possible consequences for the charge-carrier mobilities are discussed.

DOI: 10.1103/PhysRevB.75.195219 PACS number(s): 71.20.Rv, 63.20.−e, 61.66.Hq, 33.20.Ea

I. INTRODUCTION

In recent years, organic semiconductors have attracted strong interest as promising materials for future electronic and optoelectronic devices including organic field-effect transistors (OFETs),[1–5] organic light-emitting diodes,[6,7] and organic solar cells.[8,9] Apart from π-conjugated polymers, an important class of such materials is crystals that are built up from small organic molecules. These organic molecular crystals can be vapor grown with very high purity which results in charge-carrier mobilities that are orders of magnitudes larger than those of disordered polymers.[5] Prototypical examples of organic molecular crystals with high electron and/or hole mobilities are oligoacene crystals, i.e., naphthalene,[10,11] anthracene,[12,13] tetracene,[14,15] and pentacene crystals.[16–20] More recently, OFET measurements on rubrene crystals have been reported to show extremely high room-temperature mobilities.[21,22] The search for other organic materials with similar or even better transport properties is ongoing.[5]

Organic molecular crystals are bound typically by weak intermolecular interactions. Therefore, the charge transport through these crystals is mainly facilitated by π stacking of the individual molecules along certain crystallographic directions. For example, the high mobilities in oligoacene crystals are a direct consequence of the so-called herringbone stacking. Another material that exhibits this particular arrangement of its molecular constituents is crystalline durene. While durene crystals are commonly used as host crystals for high-resolution optical spectroscopy of various guest molecules,[23] it has remained relatively unknown to the field of organic electronics. On the other hand, there are indications that high-quality crystals of durene may show promising charge-carrier mobilities as well.[24,25]

The durene molecule (1,2,4,5-tetramethylbenzene) is derived from the benzene molecule by substitution of four hydrogen atoms with four methyl groups. It exhibits D_{2h} point group symmetry. The crystalline phase of durene belongs to the space group $P2_1/c$ (C_{2h}^5) with two molecules in a monoclinic unit cell (cf. Fig. 1). The herringbone stacking of the durene molecules is visible by viewing along the a^* direction, which is perpendicular to the bc plane (see Fig. 2).

In the 1970s, the crystal structure of deuterated durene has been determined by means of x-ray analysis[26] and neutron diffraction.[27] More recently, inelastic-neutron-scattering (INS) experiments have been performed by Plazanet *et al.*, and a comparison with computed spectra has been made.[28] Early studies of the vibrational properties of durene crystals were done by Raman spectroscopy, mostly in the broader context of analyzing dephasing effects in solids.[29,30] In a very recent study, INS, Raman, and infrared (IR) spectra have been recorded.[31] The theoretical analog to vibrational spectroscopy is computational spectroscopy. Simulating vibrational spectra is a valuable tool for the interpretation of the experimental ones. For example, in Ref. 31, the experimental data were supplemented by density-functional theory (DFT) calculations for intramolecular vibrational modes by employing the B3LYP functional.

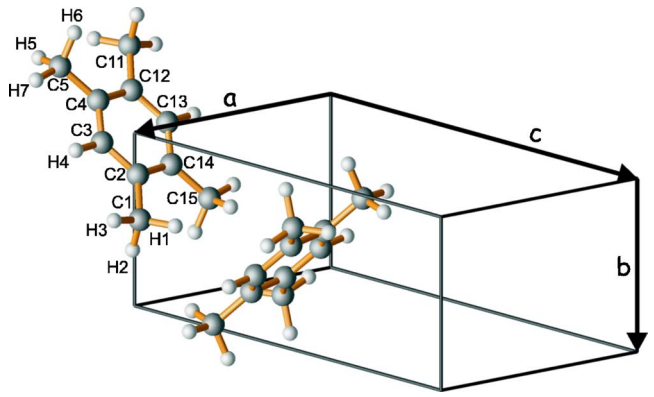

FIG. 1. (Color online) Nomenclature for carbon (C) and hydrogen (H) atoms. The lattice vectors $\boldsymbol{a}$, $\boldsymbol{b}$, and $\boldsymbol{c}$ define the monoclinic cell of a durene crystal.

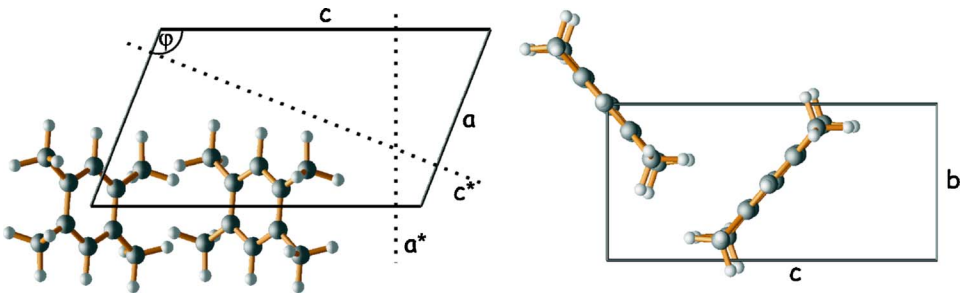

FIG. 2. (Color online) Unit cell of the durene crystal with atomic basis in a view along the vectors $\boldsymbol{b}$ (left) and $\boldsymbol{a}^*$ (right).

In the present paper, we perform a theoretical analysis of the structural, vibrational, and electronic properties of durene. In order to gain deeper insight into the various material properties, we perform all studies for a single durene molecule as well as crystalline durene. We provide a complete description of all phonon modes including a group-theoretical analysis. Moreover, we present *ab initio* IR spectra not only for the crystalline phase of durene but also for its gas phase. The comparison of the frequencies and atomic movements of the intramolecular vibrations for gas-phase species vs molecules in a crystal is used to study the strength and origin of the intermolecular interaction within the crystal. While organic molecular crystals are usually considered as purely van der Waals bonded, there are hints in the recent literature[31] that in durene crystals, significant contributions to the binding energy may come from weak intermolecular hydrogen bonds of the C-H$\cdots\pi$ type. Since the frequencies of the corresponding C-H stretching modes may significantly change upon crystallization of the molecules,[32,33] computational spectroscopy is used to detect such hydrogen bonds.

From a theoretical point of view, molecular crystals are one of the most difficult systems to simulate with *ab initio* methods. This is due to the delicate balance of equal accuracy for different strengths of bonding types, which has to be found at acceptable costs. This holds in particular for the interplay between strong *intramolecular* covalent bonds vs much weaker *intermolecular* van der Waals and possibly hydrogen bonds. An appropriate method to describe these complex materials is the DFT in conjunction with a plane-wave basis set. Moreover, the same computational apparatus can also be used to calculate accurately the properties of single molecules, i.e., the gas-phase properties, as has been recently demonstrated for other organic molecules.[32,34] Here, we will use the DFT approach to describe both phases of durene.

The paper is organized as follows. After this introduction, we describe in Sec. II the theoretical concepts and computational methods used in the present work. In Sec. III, we present and discuss our findings for the structural, vibrational, and electronic properties of durene. All calculations are performed for both the gas phase as well as the crystalline phase. We conclude the paper by a short summary in Sec. IV.

II. COMPUTATIONAL METHODS

A. Structural relaxation and total energy

When comparing molecular properties in different phases by theoretical means, the concepts applied for the modeling of each phase are important. Different methods may lead to deviations among the phases not caused by the characteristics of the structures but by inherent specifics of the computational methods. In our studies, we treat both phases of durene equally, applying the exact same concepts in order to avoid such artificial traces of the methods.

In order to determine the total energy and its minimum with respect to the atomic coordinates, we apply the DFT code Vienna *ab initio* simulation package[35,36] (VASP) using the projector augmented wave method[37] for the description of the electron-ion interaction for both the crystalline phase and the gas phase. The geometry optimization is achieved through a conjugate gradient algorithm minimizing the Hellmann-Feynman forces. Thereby residual forces are relaxed below 0.1 meV/Å. The wave functions in the interstitial region between the cores are smooth and can be expanded into a plane-wave basis set with an energy cutoff of 37 Ry. This value has been proven previously to give converged results for a variety of organic molecules.[32,34,38] Furthermore, for the calculations of crystalline durene, we have also checked the convergence of the stress tensor with respect to the energy cutoff. For test purposes, we increased the cutoff to 66 Ry where we observed small changes in the lattice constants as one might expect for soft matter, but the changes were of only minor importance.

The unit cell parameters of crystalline durene, as obtained from neutron-diffraction measurements,[28] serve us as initial coordinates for the structural relaxation. During this process, both the lattice parameters and the atomic basis are optimized. The symmetry is kept fix as space group $P2_1/c$ (C_{2h}^5). The Brillouin-zone sampling is performed using the Monkhorst-Pack scheme[39] with grid dimensions of $8\times8\times4$.

In order to simulate the gas phase, i.e., a single durene molecule, within our framework we employ a supercell approach. Thereby the molecule is placed in an orthorhombic supercell and oriented perpendicular to the cell axes in correspondence to its D_{2h} symmetry. In order to model the gas phase accurately, we have to avoid artificial interactions with neighboring cells. Since the size of the supercell determines the vacuum region between a molecule and its images, we use a rather large cell with dimensions of $24\times22\times18$ Å^3. For such large cells, the dispersion of the energy levels in the Brillouin zone is negligible and the **k**-space integration can be restricted to the Γ point.

B. Treatment of exchange and correlation effects

In order to compare the molecular and crystal properties of durene, we have to model both the intramolecular and

intermolecular interactions with equally high accuracy. This puts a high demand on the approximation of the exchange-correlation (XC) functional. Currently, there is no functional that meets this condition at acceptable computational costs. Many density functionals have been developed in the past years, each of which has its own characteristics. Here, we apply the local density approximation (LDA), the generalized gradient approximation (GGA), and a semiempirical van der Waals corrected GGA (GGA+vdW).

For the LDA calculations, we use the parametrization of Perdew and Zunger.[40] For the GGA calculations, we employ the PW91 functional[41] in order to estimate the influence of the density gradient contributions to the XC energy which are not present in LDA. Improvements over LDA are known for the simulation of strong hydrogen bonds[42] and a variety of quantities such as cohesive energies.[43] However, it is also known that the GGA approach shows deficiencies for van der Waals (vdW) bonded systems such as graphite,[44,45] which is much better described in LDA. In particular, for interacting molecules, the semilocal approximations for XC (such as GGA) fail to correctly account for the long-range attraction by vdW forces. Even if the impact on the intramolecular geometry or the electronic structure is weak, this directly affects the structure and energy of such systems in the computations. It was shown that a semiempirical correction to GGA can simulate this part of the correlation energy from strongly corrugated charge-density profiles.[44,45] This GGA+vdW approach is based on additional atom-atom potentials that vanish for covalent bonding distances. We tested GGA+vdW also for the durene crystals under study here since it gave improved results for some typical van der Waals bonded systems.[44,45]

C. Vibrational properties and IR spectra

The determination of the vibrations is based on the harmonic approximation of the nuclear potential with respect to the deviation from the ground-state geometry. This approach is justified since we are not interested in anharmonic effects such as temperature dependence of the elastic constants. Without explicit symmetry considerations, each nuclear coordinate is displaced along each positive and negative Cartesian direction by a length δ. In the spirit of the adiabatic approximation, repelling forces are calculated as Hellmann-Feynman forces linearly in δ. The resulting force constant matrix is derived from a central difference scheme in accordance with the harmonic approximation. This yields a generalized eigenvalue problem of dimension $3N$ (N number of atoms). For the crystalline (gas phase) durene with two (one) molecules per unit cell, this leads to 144 (72) phonon modes at the Γ point. As a solution, one obtains $3N$ eigenvectors representing intermolecular and/or intramolecular vibrations and $3N$ eigenvalues representing the corresponding frequencies. We stress that, for the crystalline case, the intramolecular and intermolecular vibrations result from one and the same calculation.

We optimize the displacement parameter δ to ensure harmonic motion on the one hand and to minimize numerical inaccuracies on the other hand for both the gas phase and the crystalline phase. An important criterion for the quality of our simulations is the characteristics of the acoustic phonons at the Γ point, which are lattice translations with zero frequencies. The deviation from zero, which has been used as a target quantity for the determination of δ, is approximately 1 cm^{-1}. The resulting value of δ=0.05 Å is in accordance with earlier findings for other molecular systems.[46] In the case of modes that are numerically degenerate, the symmetry of the vibrations has been properly accounted for by means of an additional symmetrization procedure.

The calculated phonon modes and frequencies are also important ingredients for the calculation of IR spectra. Given the normal modes in the harmonic approximation, the intensity of the ith normal mode in an IR spectrum is obtained from the relation[47]

$$I_i \propto \left| \frac{\partial \boldsymbol{\mu}}{\partial q_i} \right|^2. \tag{1}$$

The intensities are proportional to the squares of the dynamical dipoles, i.e., the changes of the dipole moment $\boldsymbol{\mu}$ with respect to the deflection coordinates q_i of the corresponding modes.[46] We omit all prefactors since we are interested only in the relative intensities.

D. Electronic structure

Among the most important quantities of the electronic structure of organic molecular crystals are the bandwidths of the valence and conduction bands. These quantities or, in the language of tight-binding approximation,[48] the corresponding transfer integrals are highly relevant measures for the charge-carrier mobilities and contain information about their directional dependences, as well as overall values.[49,50] Another important quantity that can be obtained from band-structure calculations is the fundamental band gap (also known as the transport gap). Additionally, the optical gap, which differs from the transport gap due to excitonic effects, is of interest for absorption spectra.

The fundamental band gap E_g is defined as[51]

$$E_g = \mathrm{IP} - \mathrm{EA}, \tag{2}$$

where the ionization potential (IP) and the electron affinity (EA) are the changes in the total energy upon electron removal or electron addition, respectively,

$$\mathrm{IP} = E(N-1) - E(N), \tag{3}$$

$$\mathrm{EA} = E(N) - E(N+1). \tag{4}$$

Here, $E(N)$ denotes the total energy of the N-electron system. This approach is called the "delta self-consistent field" (ΔSCF) scheme, since it is based on three self-consistent calculations of electronic ground states. The ΔSCF approach works very well for single-particle and two-particle excitation energies of localized electronic systems, such as molecules.[34,38]

It is important to stress that the quantity E_g, as defined in Eq. (2), is not directly related to any single-particle eigenvalue of the Kohn-Sham (KS) equations[52,53] because ground-

state DFT calculations do not take into account quasiparticle effects. Nonetheless, for simplicity, the KS eigenvalues are often used for the discussion of the electronic structure of the systems under study. The energetic difference between the KS eigenvalues of the highest occupied molecular orbital (HOMO) and the lowest unoccupied molecular orbital (LUMO) defines the fundamental KS gap E_g^{KS}, which is usually smaller than the gap defined by Eq. (2). For crystalline solids, the KS eigenvalues are frequently used to discuss the band structure, motivated by the *a posteriori* observation that the wave-vector dispersion of the individual KS bands is often more or less in agreement with experimental measurements. Here, we also use the KS bands to estimate the electronic bandwidths in durene crystals. The possible narrowing of the bandwidths due to electron-phonon coupling[49] will be treated elsewhere.[54]

In contrast to the bandwidths, the interpretation of the Kohn-Sham gap E_g^{KS} is more problematic as it is often about 50% smaller than the corresponding experimental band gap for many semiconductors. Nonetheless, for convenience, the KS eigenvalues is used as a starting point for the discussion of the band gaps and as a starting point for more sophisticated band-gap computations. One of those methods is the Green function formalism, where the refinements to the KS system are expressed as self-energy corrections.[55–57] Within the GW approximation, i.e., the linear expansion of the self-energy in the screened Coulomb interaction W (G is the single-particle Green function),[55] the resulting quasiparticle shifts usually increase the calculated band gap significantly toward the experimental value.[58,59] In the present work, we avoid the computationally demanding GW calculations and obtain the transport gap of durene crystals according to the following strategy. First, we calculate both the Kohn-Sham gap E_g^{KS} and the ΔSCF gap E_g for the durene molecule. The difference between these two gaps ($\Delta E_g = E_g - E_g^{KS}$) gives us a value for the quasiparticle gap opening in durene molecules. Then, we calculate the band structure of the durene crystal on the KS level. Finally, according to the scissors-operator approximation,[60] we rigidly shift all conduction bands by the above amount ΔE_g and identify the resulting fundamental gap with the transport gap of the durene crystal. Technically speaking, we apply the scissors operator with the quasiparticle shift obtained from the molecular calculation.

For the description of absorption experiments, where neutral excitations (electron-hole pairs) are relevant, neither the KS bands nor the GW eigenvalues can be used directly. Both approaches neglect excitonic effects which are known to be important for organic crystals where the lowest-lying pair excitation (also known as the optical gap) can be several hundreds of meV smaller than the transport gap.[61] One approach often used in order to describe such two-particle excitations is the Bethe-Salpeter equation[62,63] based on the Green function method. An alternative approach to estimate the exciton binding energy (at least for molecules) at much lower computational costs is based on an occupation constrained DFT within the ΔSCF scheme. Thereby the quantity

$$E_g^{ex} = E(N; e+h) - E(N) \tag{5}$$

defines the lowest pair excitation energy. $E(N; e+h)$ is calculated relaxing the electronic states with the restriction to an occupation according to an electron-hole pair in the HOMO-LUMO. Here, we will use this approach for the calculation of the exciton binding energy in durene molecules. We note that, in contrast to the quasiparticle shifts, the molecular exciton binding energy cannot be as easily applied to the crystal excitons since the nature of the exciton may be drastically different in the crystal. This is mainly a consequence of the increased screening in a crystal compared to a single molecule. The exciton radius can be expected to be much larger in the crystal resulting in a significantly smaller exciton binding energy.

TABLE I. Lattice constants a, b, and c (Å) and monoclinic angle φ (deg) for the durene crystal in different approximations for XC. Experimental reference data are from Plazanet *et al.* (Ref. 28).

	Expt.	LDA	GGA	GGA+vdW
a	6.817	6.432	7.497	5.765
b	5.578	5.258	6.000	4.316
c	11.505	11.200	12.790	11.614
φ	112.9	111.5	113.1	111.0

III. RESULTS AND DISCUSSION

A. Atomic geometry and energetics

In Tables I–III we present structural results for crystalline durene using three different XC approximations (LDA, GGA, and GGA+vdW). In agreement with previous studies,[44,45] the intermolecular interaction is not equally well accounted for within the three approximations for XC. As a consequence, we find some differences in the lattice parameters for durene. This can be seen from Table I which lists our calculated values for the three lattice constants a, b, and

TABLE II. Intramolecular bond lengths (Å) for the durene crystal. Root mean square (rms) value with respect to experimental reference data (Ref. 28).

	Expt.	LDA	GGA	GGA+vdW
C1–C2	1.508	1.484	1.506	1.476
C2–C3	1.399	1.391	1.400	1.393
C3–C4	1.401	1.391	1.400	1.389
C4–C5	1.508	1.484	1.506	1.479
C4–C12	1.409	1.400	1.410	1.400
C1–H1	1.092	1.107	1.100	1.082
C1–H2	1.096	1.110	1.101	1.081
C1–H3	1.088	1.102	1.097	1.077
C5–H7	1.093	1.103	1.097	1.086
C5–H6	1.095	1.109	1.101	1.086
C5–H5	1.092	1.108	1.100	1.092
C3–H4	1.090	1.100	1.093	1.094
		rms	rms	rms
		0.016	0.004	0.010

TABLE III. Intramolecular bonding angles (deg) for the durene crystal. Root mean square (rms) value with respect to experimental reference data (Ref. 28).

	Expt.	LDA	GGA	GGA+vdW
H1–C1–H2	106.9	106.0	106.5	104.8
H2–C1–H3	108.3	107.9	107.9	106.4
H3–C1–H1	108.3	108.3	107.9	105.1
C2–C1–H1	111.4	111.8	111.7	112.5
C2–C1–H2	110.8	110.9	111.5	113.5
C2–C1–H3	111.0	111.7	111.2	113.8
C1–C2–C3	120.6	121.0	120.5	122.3
C1–C2–C14	120.8	120.4	121.0	118.2
C14–C2–C3	118.6	118.5	118.5	119.5
C2–C3–H4	118.7	118.6	118.5	120.1
C2–C3–C4	122.8	122.9	123.1	120.9
H4–C3–C4	118.5	118.5	118.5	119.0
C3–C4–C5	120.6	121.0	120.5	122.5
C3–C4–C12	118.5	118.6	118.5	119.6
C12–C4–C5	120.8	120.4	121.1	117.9
C4–C5–H7	110.9	111.6	111.1	116.3
C4–C5–H6	111.2	111.0	111.5	114.0
C4–C5–H5	111.6	112.2	111.8	111.8
H7–C5–H6	108.1	107.6	107.8	106.9
H6–C5–H5	106.8	106.1	106.5	102.6
H5–C5–H7	108.2	108.1	107.9	104.0
		rms	rms	rms
		0.4	0.3	2.6

c and the monoclinic angle φ. While for the latter we find deviations on the order of only 1°–2°, the former vary over a range of 20%. Noteworthy, the LDA lattice constants are only 2%–6% smaller than those found in the experiments.[28] This good accordance of theoretical and experimental lattice parameters is lost to some extent when taking gradient corrections for XC into account. In GGA, the lattice constants are overestimated by 7%–10%. Like for typical van der Waals bonded systems, the underestimation of long-range electron correlations in GGA yields incorrect lattice parameters but the effect is much less pronounced than one might have expected. This indicates that even though van der Waals interaction is very important for the occurence of a stable crystal, there are likely additional effects contributing to the bonding between the molecules. Otherwise, the GGA lattice constants would compare worse to the experimental values.

We mention that the GGA+vdW approach, which we have used successfully for graphitic systems,[44] is not able to improve GGA lattice parameters for durene but, in fact, leads to a strong underestimation of the lattice constants a and b by more than 15%. In our GGA+vdW simulations, the two molecules in each unit cell tend to arrange in a more parallel fashion compared to the GGA calculations. This enlarges the effective stacking area of π orbitals in the b direction (see Fig. 1) and, simultaneously, increases the spatial extent of the molecules in the c direction. Hence, the c lattice constant in GGA+vdW is not as severely underestimated as the a and b lattice constants but is actually very similar to the experimental one. The shortcoming of the GGA with respect to the dispersive forces appears less serious for durene than for the systems studied in the original paper. Therefore, the van der Waals forces are probably overestimated resulting in an underestimation of the lattice constants here. The reason might be that the durene crystal is not exclusively bonded by vdW forces but, as discussed below in more detail, also hydrogen bonds contribute. For such systems, the results may be improved upon modification of the semiempirical vdW correction.

In conclusion, from our findings in Table I, we state that the lattice parameters and, hence, the intermolecular interactions in durene crystals are described most reliably in LDA.

We proceed with the discussion of the intramolecular bond lengths and bond angles for crystalline durene, which are given in Tables II and III, respectively. The overall agreement between the different levels of theory and experiment is characterized by root mean square (rms) deviations with respect to the experimental data.[28] Comparing the experimental data with our theoretical results, one finds that each of the XC functionals is able to reproduce bonding distances and angles for durene correctly. For example, in LDA, the C–C (C-H) bond lengths are shorter (longer) only by approximately 1.5%. The slight underestimation (overestimation) of the C–C (C-H) bond lengths in LDA is cured by taking gradient corrections for XC into account. From the rms value in Table II, it follows that intramolecular bond lengths come out best in GGA. As expected, for purely intramolecular properties, the vdW correction gives rise to only minor changes in the GGA values. The somewhat larger deviations in the bonding angles are probably related to the change of the lattice geometry in GGA+vdW, as described above. Yet, the rms value quantifies the deviations from the experimental bonding angles to less than 3°. As for the bonding distances, the bonding angles found in GGA and LDA are in agreement with the experiment.

From Tables II and III, we conclude that the best values for the intramolecular geometry are obtained within GGA but actually all three approximations yield very similar results. This also means that since the size of the molecules is virtually independent of the treatment of XC effects, the dramatic difference in the lattice constants (see Table I) must be attributed solely to intermolecular interactions.

After having discussed the intermolecular and intramolecular properties of durene crystals separately, we turn the discussion to the influence of the intermolecular interactions on the intramolecular bonds. For this reason, we compare in Table IV the covalent bond lengths and bond angles for gas phase durene vs crystalline durene. The comparison is done in LDA because it describes the influence of the intermolecular interactions more accurately than GGA and GGA+vdW, as demonstrated above (cf. lattice constants in Table I).

The total binding energy per durene molecule in the crystal with respect to its gas-phase state is 0.87 eV. This value results from LDA calculation without zero-point vibrational energies. From our experience with mainly vdW bonded systems in LDA, we expect this value to be a lower bound for

TABLE IV. Comparison of intramolecular bond lengths (Å) and bonding angles (deg) for gas phase and crystalline durene as calculated in LDA.

	Gas phase	Crystal
C1–C2	1.486	1.484
C2–C3	1.388	1.391
C4–C12	1.398	1.400
C1–H1	1.105	1.107
C1–H2	1.105	1.110
C5–H6	1.105	1.109
C5–H5	1.105	1.108
C1–H3	1.101	1.102
C5–H7	1.101	1.103
C3–H4	1.098	1.100
H1–C1–H2	105.9	106.0
H2–C1–H3	108.0	107.9
C2–C1–H1	111.6	111.8
C2–C1–H3	111.4	111.7
C1–C2–C3	121.1	121.0
C2–C3–C4	122.6	122.9

the experimental binding energy. Several bonding effects might contribute to this energy. Among them are van der Waals interaction, electrostatic interaction due to nonvanishing quadrupole moments, and hydrogen bonding of the weak C-H$\cdots\pi$ type. Here, we focus our discussion on the latter interaction. From the literature, we anticipate for a single C-H$\cdots\pi$ bond a binding energy on the order of 40 meV.[64] Since the maximum contribution is obtained when all eight bonds have the same strength, we estimate an upper bound of approximately 0.3 eV for the binding energy due to the C-H$\cdots\pi$ bonds. As the weak C-H$\cdots\pi$ bridges may contribute significantly (up to 30%) to the total binding energy in durene crystals, one should find additional hints for the existence of these bonds. In particular, one can expect an effect on the C-H bonds, namely, a stretching due to the attraction of the proton to the phenyl ring.[33] Therefore, we examine in the following how the C-H bonds change upon crystallization of durene.

In the gas-phase durene molecule, the four out-of-plane hydrogens (H1, H2, H5, and H6) are equivalent. This is no longer the case for the crystalline phase. As seen from Table IV, the respective C-H bond lengths are clearly stretched when the molecules build up the crystal. C-H bond elongation also appears but on a smaller scale for the other hydrogens (H3, H4, and H7), which are not directly involved in any hydrogen bond. For the out-of-plane hydrogens, the effect amounts to up to 0.005 Å. Each of these four hydrogens has a different environment more or less influenced by an adjacent phenyl ring resulting in different bond lengths. The distances to a neighboring phenyl ring may either be defined as the distance between the hydrogen atom and the center of the ring or between the hydrogen atom and the nearest carbon atom in the ring.[33] Independent of the actual definition, the shortest distance to a phenyl ring is found for H6, whereas H1 has the largest one. Taking also the possible bonding angle into consideration, it is plausible that the modifications of the bond lengths of C1–H1 and C5–H5 are weaker than those of C1–H2 and C5–H6. This ordering of the bond lengthening among the four discussed C-H bonds is in agreement with the experiments,[28] and also the measured differences between them are very similar to our theoretical findings. This shows that even though LDA has some difficulties describing strong hydrogen bonds,[42] it is very successful in the case of the weak C-H$\cdots\pi$ bond. No overbinding effects as for water[42] or for amino acids[38] have been found in our studies here.

In conclusion of this section, we have seen that simulations within LDA are able to give parameters for intramolecular, as well as intermolecular bonds in good accordance to the experiment. Though the intramolecular properties come out slightly better in GGA, we emphasize that due to its accurate lattice parameters, the LDA calculations give the best overall description of durene crystals. Hence, for all further calculations and, in particular, the calculations of the vibrational modes, we proceed using only the LDA for the XC functional.

B. Vibrational properties

In Table V, we provide a complete compilation of the frequencies, symmetries, IR intensities, and mode descriptions of the vibrations of a single durene molecule (left columns) and of the intramolecular and intermolecular Γ point phonons in durene crystals (right columns). The symmetry classification has been carried out by an analysis of the modes by means of group theory. For the durene crystal, neglecting the three zero-frequency acoustic modes, the 141 optical modes can be represented as

$$\Gamma_{vib}^{cryst} = 36A_g + 36B_g + 35A_u + 34B_u. \tag{6}$$

Analogously, for the durene molecule, the 66 genuine vibrations, i.e., without the three rotations and three translations, are given as

$$\Gamma_{vib}^{mol} = 11A_g + 10B_{1g} + 5B_{2g} + 7B_{3g} + 6A_u + 7B_{1u} + 10B_{2u} + 10B_{3u}. \tag{7}$$

Here, the index g (u) means even (odd) symmetry. Since the ground state has even symmetry, only vibrations with odd symmetry may contribute to the IR signal according to Eq. (1), whereas only vibrations with even symmetry contribute to the Raman spectra. For the mode descriptions in Table V, the usual notation for stretching (str), bending (bend), umbrella (umbr), wagging (wagg), rocking (rock), and torsion (tors) is used.

In both phases, we observe virtually the same ordering of the vibrations: starting with C-H stretching modes in the high-frequency region (2900–3100 cm^{-1}), then an intermediate region without any modes (1650–2900 cm^{-1}), and finally a vibration-rich low-frequency region (below 1600 cm^{-1}) down to the methyl group rotations (CH_3 tors) and out-of-plane bending vibrations (below 200 cm^{-1}). In the crystalline phase, we additionally obtain the nine intermo-

TABLE V. Phonon modes for the durene gas phase molecule and the durene crystal with frequencies (in cm^{-1}), symmetry classification, and relative IR intensities. The intensity of the peak maximum is set to 1000. Mode descriptions hold for all subsequent empty lines. For abbreviations, see main text.

Gas phase			Crystal			
Frequency	Symmetry	Intensity	Frequency	Symmetry	Intensity	Mode description
3069.3	A_g	0	3057.5	A_g	0	C–H str (CH)
3066.7	B_{2u}	356	3057.0	B_g	0	
			3053.7	A_u	10	
			3053.1	B_u	9	
3051.5	A_g	0	3037.1	A_g	0	C–H str (CH_3)
3051.4	B_{2u}	437	3036.6	A_u	11	
3051.4	B_{3u}	6	3034.7	B_g	0	
3051.3	B_{1g}	0	3034.3	B_u	12	
			3027.6	B_g	0	
			3027.3	A_g	0	
			3025.1	B_u	15	
			3024.9	A_u	17	
2992.1	B_{3g}	1	2974.3	A_g	0	C–H asym str (CH_3)
2992.1	A_u	1	2973.7	B_g	0	
2982.3	B_{1u}	377	2973.5	A_u	12	
2982.1	B_{2g}	0	2973.1	B_u	18	
			2963.2	A_g	0	
			2963.0	B_g	0	
			2963.0	A_u	97	
			2962.6	B_u	120	
2942.1	B_{2u}	138	2920.2	B_u	69	C–H_3 symm str
2941.8	B_{1g}	0	2919.4	B_g	0	
2937.6	A_g	0	2918.9	A_u	102	
2936.7	B_{3u}	1000	2918.5	A_g	0	
			2912.5	B_g	0	
			2911.9	A_g	1	
			2911.3	A_u	235	
			2911.1	B_u	271	
1646.2	B_{1g}	0	1630.9	A_g	0	C–C str (ring def.), C–H bend in plane
			1630.0	B_g	0	
1587.8	A_g	0	1580.3	B_g	0	C–C str (ring def.)
			1578.4	A_g	0	
1509.4	B_{3u}	347	1503.2	A_u	48	C–C str (ring def.), C–H bend in plane
			1501.6	B_u	34	
1456.7	B_{2u}	377	1447.8	A_u	23	C–C str (ring def.), CH_3 bend
			1445.0	B_u	26	
1419.4	B_{3u}	34	1422.2	B_u	4	C–H_3 bend
1407.4	A_g	0	1417.5	B_g	0	
1402.9	B_{1u}	442	1406.6	A_u	44	
1401.6	B_{2g}	0	1402.7	A_g	0	
1389.9	B_{1g}	0	1393.5	B_g	0	
1387.0	B_{3g}	0	1392.7	A_g	0	
1386.8	A_u	0	1391.1	B_u	9	
			1390.9	B_g	0	
			1385.0	A_g	0	

TABLE V. (*Continued.*)

Gas phase			Crystal			
Frequency	Symmetry	Intensity	Frequency	Symmetry	Intensity	Mode description
			1379.9	A_u	12	
			1376.9	B_u	10	
			1376.7	B_g	0	
			1374.2	A_u	0	
			1371.5	A_g	0	
			1368.9	A_u	28	
1367.6	B_{3u}	26	1364.1	B_u	151	C–C str (ring def.), CH_3 bend
			1359.9	A_u	40	
1365.3	B_{2u}	124	1354.4	B_u	30	CH_3 bend, C–C str (ring def.)
1338.6	A_g	0	1344.3	B_g	0	CH_3 umbr
1326.7	B_{3u}	132	1332.4	B_u	60	
1322.9	B_{1g}	0	1320.6	A_g	0	
1322.9	B_{2u}	97	1319.2	B_u	111	
			1319.0	A_g	0	
			1317.6	A_u	1	
			1311.8	B_g	0	
			1303.4	A_u	22	
1297.2	A_g	0	1292.0	B_g	0	C–C str (ring breath.), CH_3 umbr, $C-CH_3$ str
			1290.3	A_g	0	
1232.2	B_{1g}	0	1233.9	B_g	0	C–H bend in plane
			1232.4	A_g	0	
1195.9	B_{2u}	1	1201.9	B_u	265	$C-CH_3$ str, C–C bend in plane (ring def.)
			1201.3	A_u	3	
1176.3	B_{3u}	0	1175.7	A_u	225	C–H bend in plane
			1174.1	B_u	43	
1093.4	B_{1g}	0	1093.5	A_g	0	$C-CH_3$ str, C–C bend in plane (ring def.)
			1092.1	B_g	0	
1013.8	A_u	0	1019.5	A_g	0	$C-H_3$ wagg
1013.5	B_{3g}	0	1017.4	A_u	23	
			1016.8	B_g	0	
			1014.7	B_u	26	
1002.8	B_{1g}	0	1005.4	B_g	0	$C-H_3$ rock
			1004.6	A_g	0	
989.5	B_{1u}	128	991.5	B_u	102	$C-H_3$ wagg
973.7	B_{2g}	0	990.9	A_u	36	
			983.1	B_g	0	
			981.8	A_g	0	
973.7	B_{3u}	287	975.0	A_u	54	$C-H_3$ rock
954.4	A_g	0	974.3	B_u	262	
950.8	B_{2u}	8	958.9	B_g	0	
			957.9	A_g	0	
			953.6	B_u	31	
			952.0	A_u	20	
860.1	B_{3g}	0	876.1	B_g	0	C–H wagg

TABLE V. (*Continued.*)

Gas phase			Crystal			
Frequency	Symmetry	Intensity	Frequency	Symmetry	Intensity	Mode description
846.6	B_{1u}	112	874.5	A_g	0	
			849.9	A_u	140	
			844.5	B_u	52	
818.5	B_{3u}	5	820.8	B_u	553	C–CH_3 str, C–C str
			814.9	A_u	164	
748.3	A_g	0	751.1	A_g	0	C–C bend (ring def.)
			747.7	B_g	0	
711.9	B_{3g}	0	714.4	B_g	0	C–C bend out of plane
			712.7	A_g	0	
668.9	B_{2u}	6	674.2	B_u	56	C–CH_3 str, C–C bend
			673.3	A_u	62	
580.7	A_u	0	584.7	B_u	30	C–C bend out of plane
			582.3	A_u	37	
			515.8	B_g	0	C–C bend (ring def.)
509.5	B_{1g}	0	514.9	A_g	0	C–CH_3 bend
			513.9	B_g	0	
507.6	A_g	0	510.8	A_g	0	C–C bend (ring def.)
443.8	B_{1u}	59	444.3	A_u	204	C–C bend out of plane
			443.1	B_u	304	
425.2	B_{1g}	0	431.9	B_g	0	C–C bend (ring def.)
			428.8	A_g	0	
328.9	B_{2g}	0	345.8	A_g	0	C–CH_3 wagg
			341.8	B_g	0	
296.0	B_{3u}	5	316.2	A_u	2	C–CH_3 bend
285.1	B_{2u}	7	314.5	B_u	62	
277.0	A_g	0				
264.7	B_{3g}	0	304.6	B_g	0	C–CH_3 wagg
			301.7	A_g	0	
			294.9	A_g	0	C–CH_3 bend
			294.9	A_u	5	
			293.1	B_u	23	
			290.5	B_g	0	
181.0	B_{1u}	13				CH_3 tors, C–CH_3 wagg
			224.8	A_u	262	Butterfly
141.9	B_{2g}	0	219.0	A_g	0	CH_3 tors
			218.2	B_g	0	
			214.3	B_u	451	Butterfly
122.3	A_u	0	201.0	B_u	18	CH_3 tors
111.3	B_{3g}	0	193.6	A_u	21	
			186.9	A_g	0	
			186.4	A_u	3	
110.6	B_{1u}	45				Butterfly
106.6	A_u	0	180.2	B_u	30	C–CH_3 wagg, CH_3 tors
			175.2	A_u	5	C–CH_3 wagg
			173.7	B_g	0	CH_3 tors
			163.1	B_u	4	

TABLE V. (*Continued.*)

Gas phase			Crystal			
Frequency	Symmetry	Intensity	Frequency	Symmetry	Intensity	Mode description
			140.2	A_g	0	R_{CH}
			140.2	B_g	0	
			120.7	A_g	0	R_L
			113.2	B_g	0	
			102.4	A_u	1000	T_c
			84.0	B_u	10	T_b
			61.7	A_g	0	R_6
			53.2	A_u	0	T_a
			51.5	B_g	0	R_6

lecular vibrations (below 150 cm^{-1}), classified as three translations (T) basically along the lattice vectors $\boldsymbol{a}$,$\boldsymbol{b}$, and $\boldsymbol{c}$ and six librations, i.e., molecule rotations (R) about the axes corresponding to the principal moments of inertia. The rotating axis related to the R_6 rotation is perpendicular to the plane of the phenyl ring, whereas the axis corresponding to R_L (R_{CH}) lies in the plane and is the long (short) axis of the molecule. More precisely, the R_{CH} axis points in the direction of the C3–H4 bond (cf. Fig. 1) and the R_L axis is perpendicular to it. The six librational normal modes have even symmetry, i.e., they are not IR active, whereas the three translational modes belong to u representations and should have more or less strong transition dipole moments.[65]

The IR intensities in Table V are calculated according to Eq. (1) and normalized to a peak maximum of 1000, separately for the gas phase and the crystal. The normalized IR intensities are subsequently converted into IR spectra applying a line broadening of 5 cm^{-1}. The resulting IR spectra are plotted in Fig. 3 for gas-phase molecules (top panels) and for crystals (bottom panels). We note that, in agreement with the above symmetry arguments, only the modes with odd symmetry are visible in our calculated IR spectra. In fact, the few nonvanishing but extremely small intensities for even modes (e.g., B_{3g}, 2992.1 cm^{-1}, intensity of 0.7) can be regarded as residual transition dipole moments and are a measure for the high accuracy of our method.

First, we discuss the similarities and differences in the IR spectra of both phases. Concerning the overall intensities, we observe a considerable redistribution of spectral weights when durene condenses, albeit the bonding in the crystal has no ionic or covalent contribution. For the molecule, the largest IR intensities are seen for C-H and C-H_3 stretching

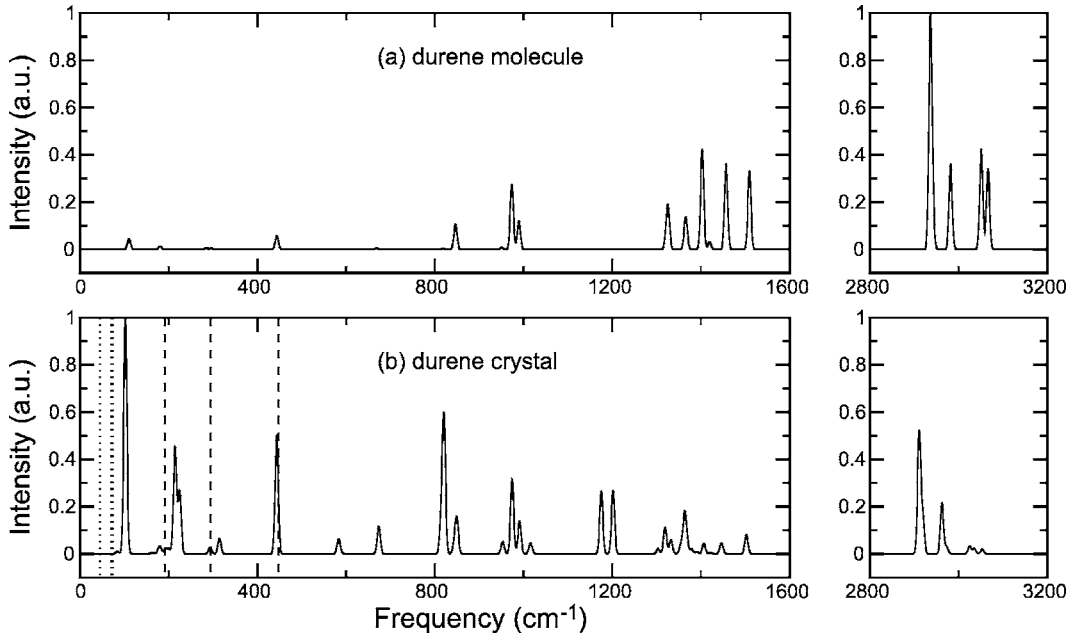

FIG. 3. Infrared spectra of durene gas phase molecule (upper panel) and durene single crystal (lower panel) normalized to the respective peak maxima. Experimental low-frequency intramolecular (dashed lines) and intermolecular modes (dotted lines) as taken from Refs. 31 and 65, respectively, are indicated.

modes in the high-frequency region, whereas for the crystalline phase, the strongest peaks appear in the lower part of the spectrum. In solid durene, the most pronounced IR peak belongs to an intermolecular translational vibration (T_c) that has no counterpart in the molecular spectrum. Next to it, we observe a second strong feature of the durene crystal, namely, a double peak that originates from a butterfly mode (with dominating C-CH_3 out-of-plane wagging contribution) split into an A_u mode at 225 cm^{-1} and a B_u mode at 214 cm^{-1}. For the molecule, however, this mode appears at 111 cm^{-1}, i.e., at about half the wave number in comparison to crystalline durene. This effect caused by the intermolecular interaction is also observed for other phonon modes in the low-frequency region where the wave numbers are generally blueshifted with respect to their counterparts for the corresponding modes in the molecule. This is not astonishing, since the strength of intermolecular interactions becomes more important for modes with smaller force constants or larger effective masses. As a consequence, the shape of the nuclear potential in the presence of adjacent molecules in the crystal environment is changed yielding different normal modes and shifted frequencies. In contrast, higher-frequency modes are much less affected and, in fact, above 400 cm^{-1} the vibrational frequencies of both durene phases become very similar, with the differences being a few cm^{-1} for most of the modes and rarely above 20 cm^{-1}.

In recent experimental IR studies on the vibrational properties of durene, the low-frequency region has been investigated at up to 600 cm^{-1}.[31] The spectrum exhibits three peaks originating from intramolecular phonons which are indicated as dashed lines at the respective energies in Fig. 3(b). The main peak is at 447 cm^{-1} and another peak with nearly equal height but larger linewidth is seen at 191 cm^{-1}. A smaller peak appears at 294 cm^{-1}. Each of the peaks mentioned can be seen in our calculations as well. The first one corresponds to C-C out-of-plane bending vibrations related to a nearly degenerate pair of modes at around 444 cm^{-1}. The second peak comes from the above-mentioned butterfly modes. Due to the splitting of 11 cm^{-1}, this feature is smaller in the IR spectrum than the first peak [see Fig. 3(b)] though larger transition dipole moments are involved. This explains the larger linewidth seen in the experimental spectrum. The third and smallest experimental peak at 294 cm^{-1} reappears in our calculated spectrum with a low relative intensity at 315 cm^{-1}. Hence, for this spectral range, measurements and theoretical predictions agree very well.

Besides the aforementioned spectral features, we see a very pronounced peak at 102 cm^{-1} in the region of the intermolecular phonons. This peak is not seen in IR spectra from suspension[31] but the translational modes are seen in the spectra of single crystals.[65] We note that in the latter experiments the peak positions change upon cooling the crystals from room temperature down to 80 K. In Fig. 3(b), we have plotted the experimental frequencies at 80 K as dotted lines. At that temperature, the T_b (T_a) translation is found at 70(45) cm^{-1} which is in surprisingly good accordance with our findings of 84(53) cm^{-1}. Even for the T_c mode, the value of 102 cm^{-1} accords reasonably well with the experimental wave number of 74 cm^{-1}.

From Table V, a direct comparison of the high-frequency vibrational modes of both phases is possible and allows us to further elaborate on our discussion of a possible C-H$\cdots\pi$ bond. This can be done by comparing the C-H stretch motions of aromatic C-H bonds and methyl group C-H stretching vibrations. In general, the frequency lowering upon condensation is observed in the range of 10–25 cm^{-1}. This is a very small wave-vector shift even for a weak hydrogen bond,[33] and it shows that we are possibly dealing with the weakest form of such a bond. The aromatic C-H groups give rise to the smallest shifts of approximately 10 cm^{-1}, whereas the methyl C-H stretching vibrations are more affected, thus indicating a hydrogen donor. For the latter modes, which are under suspicion of an influence of a weak C-H$\cdots\pi$ bond, the average redshift amounts to about 20 cm^{-1}. This is neither a strong argument for the hydrogen bond nor against it, but at least it is an indication of such a bond. To our knowledge, unfortunately, there is no experimental data for comparison on that point. There are data for polycrystalline samples,[30] but the deviations between theory and experiment clearly exceed the relevant energy range.

Finally, we turn our attention to the modes with g symmetry which are not visible in the IR signal but in Raman measurements. The Raman spectrum of powder samples of durene[31] shows a major contribution from the spectral region below 150 cm^{-1} Correspondingly, in our calculations from Table V, we find such modes between 110 and 140 cm^{-1} associated with librations. Furthermore, the experimental Raman frequencies[31] in the range of 250-1650 cm^{-1} are also well reproduced by the calculations.

C. Electronic properties

In Fig. 4, we have plotted the band structure of durene crystals (left) in comparison to the energy levels in durene molecules (right). All values were obtained as eigenvalues of the Kohn-Sham equation, as discussed in Sec. II D. We use the notation of high-symmetry points, as depicted in the sketch of the irreducible part of the Brillouin zone in Fig. 5. The most important high-symmetry lines are ΓB along the a^* direction, ΓY along the b direction, and ΓZ along the c^* direction [the latter is defined as being perpendicular to the ab plane (see Fig. 2)]. Figure 4 also shows isodensity plots of crystal and molecular orbitals for the highest occupied crystal orbital (HOCO) and the HOMO, respectively.

The bands are formed by delocalized π orbitals of the molecule. Since the crystal unit cell contains two molecules, there are twice the number of states per unit cell in comparison to the gas phase species. At Γ, the HOCO and the HOCO-1 are similar to the HOMO as seen from the insets in Fig. 4. The same analogy holds for the states below, namely, the HOCO-2 and HOCO-3 which are formed from the HOMO-1. The identification of the hole states with former molecular orbitals is justified by visual identification on the one hand and the correspondence of the energy levels on the other hand. From Fig. 4, it is obvious that the energetic positions of molecular orbitals experience changes below 1 eV when transforming into Bloch states in the crystal; thus, the energetic ordering is comparable to the energy structure in the molecule. Of course, a rather strong band dispersion occurs due to the intermolecular interaction. Investigating the

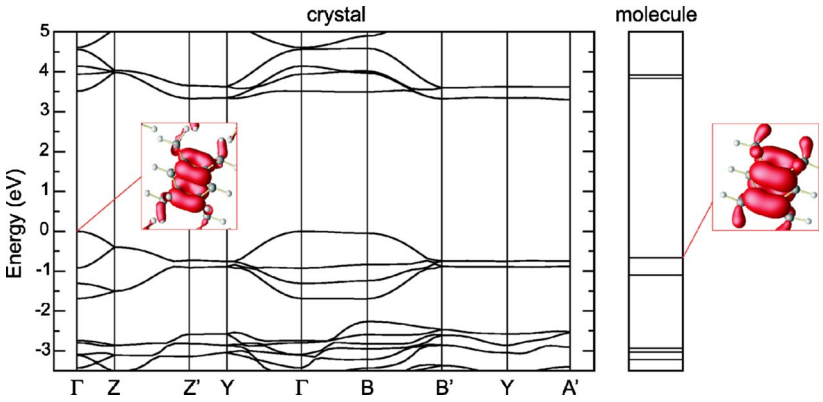

FIG. 4. (Color online) Band structure of durene along special lines in the Brillouin zone (left) in comparison to molecular energy levels (right). The valence-band maximum is set to zero. For the definition of the high-symmetry points, see Fig. 5. The absolute squares of the wave functions of the HOCO and the HOMO are depicted in the insets.

states in the conduction band, a correspondence between molecular orbitals and crystal orbitals, established by their characteristic shapes (not shown in Fig. 4), can be obtained as well.

For the valence bands, i.e., for the holes, we find a rather strong wave-number dispersion for the HOCO/HOCO-1 resulting in a large bandwidth. The bandwidth can be quantified by the band splitting at Γ, which is mainly due to the interaction of both molecules in a crystal unit cell. The splitting amounts to 0.92 eV yielding a large transfer integral. Similarly, the HOCO-2/HOCO-3 exhibits a strong dispersion with a splitting of 0.38 eV at Γ. The total splitting at Γ (HOCO/HOCO-3) amounts to 1.69 eV. These values give rise to bandwidths that are unusually large for an organic molecular crystal and indicate potentially high hole mobilities in durene crystals.

The valence-band dispersion, however, is extremely anisotropic. We find a very strong dispersion in the b (ΓY) direction and in the c^* (ΓZ) direction for the HOCO/HOCO-1, as well as for the HOCO-2/HOCO-3. This is easily understood since there is a strong wave-function overlap from the two molecules in the unit cell within the bc plane and of adjacent molecules belonging to different unit cells in the b direction (see Fig. 2). The overlap is directly influenced by the spatial extent of the molecular orbitals. This extent is maximized in two directions: along the R_6 axis and along the long axis R_L of the molecule both of which are within the bc plane. In the insets of Fig. 4, this is visible for the bonds to the out-of-plane hydrogens carrying charge density from the

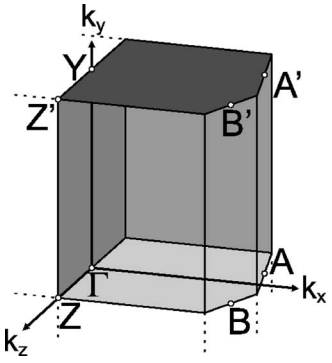

FIG. 5. Irreducible wedge of the Brillouin zone of a durene crystal. Important high-symmetry lines: ΓB along $\boldsymbol{a}^*$, ΓY along $\boldsymbol{b}$, and ΓZ along $\boldsymbol{c}^*$.

HOMO (HOCO). As a direct consequence, large transfer integrals occur in the bc plane. Smaller transfer integrals and, hence, smaller dispersion are observed in the a^* (ΓB) direction. This anisotropic behavior becomes evident from the geometry in Fig. 2. The a^* direction is perpendicular to the bc plane and parallel to the planes of the aromatic rings of both molecules; e.g., the herringbone fashion is visible along the vector $\boldsymbol{a}^*$. In that direction, the π-orbital overlap of adjacent molecules is minimized, whereas along $\boldsymbol{b}$ or $\boldsymbol{c}^*$, a band can be formed effectively. This is similar to another group of herringbone stacked organic molecular crystals, namely, the polyacenes. From these findings, we expect very anisotropic hole mobilities.[49,50] The hole mobility should be minimal in the a^* direction, whereas high mobilities are expected to occur within the bc plane.

For the conduction bands, i.e., the electron states, similar effects are observed. The bands formed from the two lowest unoccupied molecular orbitals (LUMO and LUMO+1) overlap since the dispersion is much larger than the energy difference of 0.1 eV between LUMO and LUMO+1. The corresponding total splitting (LUCO-LUCO+3) at Γ is 1.05 eV, which also indicates possibly high electron mobilities in durene crystals. Furthermore, Fig. 4 exhibits the same characteristic anisotropy for the electrons as found for the holes.

Crystalline durene represents an indirect semiconductor. The maximum of the occupied bands occurs at Γ, whereas the minimum of the empty bands is situated at A'. The KS gap, as calculated in Fig. 4, amounts to 3.3 eV and is reduced considerably compared to the HOMO-LUMO gap of 4.5 eV in the molecule. This reduction is mainly due to the formation of bands with relatively strong dispersion. The direct KS gap in the crystal is found at Γ and amounts to 3.5 eV.

As discussed in Sec. II, the Kohn-Sham (HOMO-LUMO) gap presented here may not be directly identified with the energy of the lowest electronic pair excitation of the system. In order to give energies which can be compared to experimental transport gaps, we augment the KS values with a quasiparticle shift according to the method described above. From gas-phase calculations, the quasiparticle gap according to Eq. (2) is determined to be 7.9 eV, resulting in a quasiparticle shift of 7.9−4.5=3.4 eV. Hence, the indirect gap of the durene crystal including this shift is estimated to be 3.3 +3.4=6.7 eV.

Finally, we have calculated the optical gap E_g^{ex} according to Eq. (5) and found a value of 4.6 eV for the single mol-

ecule. This corresponds to a large exciton binding energy of 7.9−4.6=3.3 eV. As explained in Sec. II D, this value cannot be directly applied to crystal excitons. Instead, a solution of the Bethe-Salpeter equation similar to Ref. 57 would be necessary to calculate excitonic effects in durene crystals. This, however, is beyond the scope of the present paper.

IV. SUMMARY

We have investigated various material properties of durene molecules and durene crystals by means of density-functional theory. Both phases of durene have been treated on equal footing using a projector-augmented wave scheme in conjunction with a plane-wave basis set and periodic boundary conditions. This approach has allowed us to model both the intramolecular and intermolecular interactions equally well and made a detailed comparison of the molecular and crystal properties of durene feasible.

First, we have calculated the atomic equilibrium geometries using several exchange and correlation functionals (LDA, GGA, and GGA+vdW). From a comparison with experimental data, we conclude that the *intermolecular* interactions in durene crystals are described most reliably in LDA which underestimates the experimental lattice constants by only 2%–6%. The *intramolecular* geometries are found to be very similar in all three approximations and the overall agreement with experiment is very good; e.g., the deviations in LDA are about 1.5% for bond lengths and less than 0.5% for bond angles. Furthermore, from the comparison of the covalent bonds in gas phase durene vs crystalline durene, we have found indications that not only van der Waals interactions but also weak C-H$\cdots\pi$ hydrogen bonds stabilize the crystalline phase.

In a second step, we have determined the vibrational frequencies and eigenmodes of both phases. A symmetry classification by means of group theory has been performed in order to identify IR-active and Raman-active modes. Additionally, complete IR spectra have been calculated for isolated molecules as well as crystals of durene. For those phonon modes where experimental data are available, we have observed a good correspondence between measured IR signals and our LDA calculations.

Finally, we have calculated the electronic properties, i.e., the band structure of durene crystals and the corresponding energy levels in gas-phase durene molecules. Even though the intermolecular forces are relatively weak, there are considerable changes in the electronic structure upon crystallization. We observe a rather strong dispersion of the highest valence bands, as well as the lowest conduction bands. The corresponding splittings at the Γ point which is indicative of the bandwidths are found to be 1.69 and 1.05 eV, respectively. However, the band dispersions are found to be extremely anisotropic with large transfer integrals for the b and c directions and rather small dispersions along the a^* direction. We have traced back this behavior to the fact that there is a large wave-function overlap (π stacking) from neighboring molecules within the bc plane, whereas the π-orbital overlap is minimized along the a^* direction. From our findings, we expect rather large but highly anisotropic charge-carrier mobilities in durene crystals.

ACKNOWLEDGMENTS

We would like to thank the Deutsche Forschungsgemeinschaft for financial support (Project HA 2900/3-2). This work was supported by the European Community within the framework of the Network of Excellence NANOQUANTA (Contract No. NMP4-CT-2004-500198). Grants for computer time from the Leibniz-Rechenzentrum München and the Höchstleistungsrechenzentrum Stuttgart are gratefully acknowledged.

[1] A. R. Brown, A. Pomp, C. M. Hart, and D. M. de Leeuw, Science **270**, 972 (1995).
[2] A. Dodabalapur, L. Torsi, and H. E. Katz, Science **268**, 270 (1995).
[3] H. Sirringhaus, N. Tessler, and R. H. Friend, Science **280**, 1741 (1998).
[4] M. Muccini, Nat. Mater. **5**, 605 (2006).
[5] M. E. Gershenson, V. Podzorov, and A. F. Morpurgo, Rev. Mod. Phys. **78**, 973 (2006).
[6] M. Berggren, O. Inganäs, G. Gustafsson, J. Rasmusson, M. R. Andersson, T. Hjertberg, and O. Wennerstrom, Nature (London) **372**, 444 (1994).
[7] A. J. Heeger, Solid State Commun. **107**, 673 (1998).
[8] M. Granström, K. Petritsch, A. C. Arias, A. Lux, M. R. Andersson, and R. H. Friend, Nature (London) **395**, 257 (1998).
[9] S. E. Shaheen, C. J. Brabec, N. S. Sariciftci, F. Padinger, T. Fromherz, and J. C. Hummelen, Appl. Phys. Lett. **78**, 841 (2001).
[10] W. Warta and N. Karl, Phys. Rev. B **32**, 1172 (1985).
[11] K. Hannewald and P. A. Bobbert, Appl. Phys. Lett. **85**, 1535 (2004).
[12] N. Karl, in *Semiconductors*, Landolt-Bönstein Numerical Data and Functional Relationships in Science and Technology (New Series), Group III, Vol. 17, edited by O. Madelung, M. Schulz, and H. Weiss (Springer, Berlin, 1985), pp. 106–218.
[13] K. Hannewald and P. A. Bobbert, in *Physics of Semiconductors*, AIP Conf. Proc. No. 772, edited by J. Menendez and C. G. van de Walle (AIP, Melville, NY, 2005), p. 1101.
[14] R. W. I. de Boer, M. E. Gershenson, A. F. Morpurgo, and V. Podzorov, Phys. Status Solidi A **201**, 1302 (2004).
[15] J. Niemax, A. K. Tripathi, and J. Pflaum, Appl. Phys. Lett. **86**, 122105 (2005).
[16] J. Cornil, P. P. Calbert, and J. L. Brédas, J. Am. Ceram. Soc. **123**, 1250 (2001).
[17] V. Y. Butko, X. Chi, D. V. Lang, and A. P. Ramirez, Appl. Phys. Lett. **83**, 4773 (2003).
[18] O. D. Jurchescu, J. Baas, and T. T. M. Palstra, Appl. Phys. Lett. **84**, 3061 (2004).
[19] N. Koch, A. Vollmer, I. Salzmann, B. Nickel, H. Weiss, and J. P. Rabe, Phys. Rev. Lett. **96**, 156803 (2006).
[20] J. Y. Lee, S. Roth, and Y. W. Park, Appl. Phys. Lett. **88**, 252106

(2006).
[21] V. C. Sundar, J. Zaumseil, V. Podzorov, E. Menard, R. L. Willett, T. Someya, M. E. Gershenson, and J. A. Rogers, Science **303**, 1644 (2004).
[22] M. Fischer, M. Dressel, B. Gompf, A. K. Tripathi, and J. Pflaum, Appl. Phys. Lett. **89**, 182103 (2006).
[23] M. A. Neumann, M. R. Johnson, P. G. Radaelli, H. P. Trommsdorff, and S. F. Parker, J. Chem. Phys. **110**, 516 (1999).
[24] Z. Burshtein and D. F. Williams, Phys. Rev. B **15**, 5769 (1977).
[25] A. K. Tripathi and J. Pflaum (private communication).
[26] C. H. Stam, Acta Crystallogr., Sect. B: Struct. Crystallogr. Cryst. Chem. **28**, 2630 (1972).
[27] E. Prince, L. W. Schroeder, and J. J. Rush, Acta Crystallogr., Sect. B: Struct. Crystallogr. Cryst. Chem. **29**, 184 (1973).
[28] M. Plazanet, M. R. Johnson, J. D. Gale, T. Yildirim, G. J. Kearley, M. T. Fernández-Díaz, D. Sánchez-Portal, E. Artacho, J. M. Soler, P. Ordejón, A. Garcia, and H. P. Trommsdorff, Chem. Phys. **261**, 189 (2000).
[29] C. B. Harris, R. M. Shelby, and P. A. Cornelius, Phys. Rev. Lett. **38**, 1415 (1977).
[30] S. Marks, P. A. Cornelius, and C. B. Harris, J. Chem. Phys. **73**, 3069 (1980).
[31] A. Pawlukojć, I. Natkaniec, G. Bator, L. Sobczyk, E. Grech, and J. Nowicka-Scheibe, Spectrochim. Acta, Part A **63**, 766 (2006).
[32] R. Maul, F. Ortmann, M. Preuss, K. Hannewald, and F. Bechstedt, J. Comput. Chem. (to be published).
[33] G. R. Desiraju and T. Steiner, *The Weak Hydrogen Bond in Structural Chemistry and Biology* (Oxford University Press, NY, 1999).
[34] M. Preuss, W. G. Schmidt, K. Seino, J. Furthmüller, and F. Bechstedt, J. Comput. Chem. **25**, 112 (2004).
[35] G. Kresse and J. Furthmüller, Comput. Mater. Sci. **6**, 15 (1996).
[36] G. Kresse and J. Furthmüller, Phys. Rev. B **54**, 11169 (1996).
[37] G. Kresse and D. Joubert, Phys. Rev. B **59**, 1758 (1999).
[38] R. Maul, M. Preuss, F. Ortmann, K. Hannewald, and F. Bechstedt, J. Phys. Chem. A **111**, 4370 (2007).
[39] H. J. Monkhorst and J. D. Pack, Phys. Rev. B **13**, 5188 (1976).
[40] J. P. Perdew and A. Zunger, Phys. Rev. B **23**, 5048 (1981).
[41] J. P. Perdew, in *Electronic Structure of Solids '91*, edited by P. Ziesche and H. Eschrig (Akademie-Verlag, Berlin, 1991), p. 11.
[42] D. R. Hamann, Phys. Rev. B **55**, R10157 (1997).
[43] J. P. Perdew, J. A. Chevary, S. H. Vosko, K. A. Jackson, M. R. Pederson, D. J. Singh, and C. Fiolhais, Phys. Rev. B **46**, 6671 (1992).
[44] F. Ortmann, F. Bechstedt, and W. G. Schmidt, Phys. Rev. B **73**, 205101 (2006).
[45] F. Ortmann, W. G. Schmidt, and F. Bechstedt, Phys. Rev. Lett. **95**, 186101 (2005).
[46] M. Preuss and F. Bechstedt, Phys. Rev. B **73**, 155413 (2006).
[47] E. B. Wilson, J. C. Decius, and P. C. Cross, *Molecular Vibrations: The Theory of Infrared and Raman Vibrational Spectra* (McGraw-Hill, New York, 1955).
[48] N. W. Ashcroft and N. D. Mermin, *Solid State Physics* (Saunders, Philadelphia, 1976).
[49] K. Hannewald, V. M. Stojanović, J. M. T. Schellekens, P. A. Bobbert, G. Kresse, and J. Hafner, Phys. Rev. B **69**, 075211 (2004).
[50] K. Hannewald and P. A. Bobbert, Phys. Rev. B **69**, 075212 (2004).
[51] R. O. Jones and O. Gunnarsson, Rev. Mod. Phys. **61**, 689 (1989).
[52] P. Hohenberg and W. Kohn, Phys. Rev. **136**, B864 (1964).
[53] W. Kohn and L. J. Sham, Phys. Rev. **140**, A1133 (1965).
[54] F. Ortmann, K. Hannewald, and F. Bechstedt (unpublished).
[55] L. Hedin, Phys. Rev. **139**, A796 (1965).
[56] R. W. Godby, M. Schlüter, and L. J. Sham, Phys. Rev. Lett. **56**, 2415 (1986).
[57] P. H. Hahn, W. G. Schmidt, and F. Bechstedt, Phys. Rev. B **72**, 245425 (2005).
[58] M. S. Hybertsen and S. G. Louie, Phys. Rev. B **34**, 5390 (1986).
[59] W. G. Aulbur, L. Jönsson, and J. W. Wilkins, Solid State Phys. **54**, 1 (2000).
[60] G. A. Baraff and M. Schlüter, Phys. Rev. B **30**, 3460 (1984).
[61] J.-W. van der Horst, P. A. Bobbert, and M. A. J. Michels, Phys. Rev. B **66**, 035206 (2002).
[62] S. Albrecht, L. Reining, R. Del Sole, and G. Onida, Phys. Rev. Lett. **80**, 4510 (1998).
[63] L. X. Benedict, E. L. Shirley, and R. B. Bohn, Phys. Rev. Lett. **80**, 4514 (1998).
[64] D. Philp and J. M. A. Robinson, J. Chem. Soc., Perkin Trans. 2 **2**, 1643 (1998).
[65] A. Hadni, B. Wyncke, G. Morlot, and X. Gerbaux, J. Chem. Phys. **51**, 3514 (1969).